International Journal of Heat and Mass Transfer 118 (2018) 75–87

Contents lists available at ScienceDirect

International Journal of Heat and Mass Transfer

journal homepage: www.elsevier.com/locate/ijhmt

Experimental study of heat transfer to non-Newtonian fluids inside a scraped surface heat exchanger using a generalization method

D. Crespí-Llorens [a,*], P. Vicente [a], A. Viedma [b]

[a] Dep. Ing. Mecánica y Energía, Universidad Miguel Hernández, Av. Universidad, s/n, 03202 Elche, Spain
[b] Dep. Ing. Térmica y de Fluidos, Universidad Politécnica de Cartagena, Dr. Fleming, s/n, 30202 Cartagena, Spain

ARTICLE INFO

Article history:
Received 23 June 2017
Received in revised form 8 September 2017
Accepted 27 October 2017
Available online 22 November 2017

Keywords:
Heat transfer
Non-Newtonian
Power Law
Experimental
Enhanced heat exchanger

ABSTRACT

The heat transfer process to a non-Newtonian pseudoplastic fluid inside a scraped surface heat exchanger has been experimentally analysed. The scraping device consists of a rod with semicircular pieces mounted on it, which are in contact with the inner surface of the pipe. The whole moves axially and thus, the pieces scrape the inner surface of the pipe, in order to avoid fouling formation and enhance heat transfer.

Pressure drop, heat transfer and power consumption measurements, using non-Newtonian pseudoplastic fluids, have been carried out in static and dynamic conditions of the scraper. Four flow regions have been identified: attached laminar, detached laminar, transitional and turbulent flow regions. A generalization method for the fluid viscosity that includes the effects of the non-Newtonian behaviour has been used. Friction factor and Nusselt number have been successfully correlated by employing the generalized viscosity on pressure drop and heat transfer results, both in static and dynamic conditions, for three of the four identified flow regions (it was not possible to get correlations in the transition to turbulent flow region). The study shows that, despite the high power consumption of the scraping movement, the device is suitable for an industrial process using non-Newtonian fluids, since it prevents fouling, increases heat transfer, provides flexibility and enhances the final product quality. Furthermore, the obtained correlations are a valuable tool in the design of heat exchangers.

© 2017 Elsevier Ltd. All rights reserved.

1. Introduction

Heat exchangers in the food and chemical industries usually have low efficiency when working with non-Newtonian fluids. These fluids have high apparent viscosities and therefore, laminar flow at high Prandtl numbers usually occurs. Moreover, the fouling problem in these heat exchangers has a significant impact on heat transfer inefficiencies and on cleaning downtime [4,5]. Besides, high temperature gradients in heated fluids are common, which decreases the quality of the process and sometimes of the fluid itself.

Moving insert devices that scrape the heat exchanger surfaces can be the best option, since they solve some of the problems that may occur when smooth pipes are employed on high viscous fluids. When the heat transfer surface is scraped, the heat exchanger is not required to be oversized to take into account the heat transfer decrease due to fouling. Moving scrapers permit us to work in food or chemical processes without the need of stops that affect plant productivity. Heating a fluid which is highly mixed, produces a uniform temperature field in the fluid that improves its quality, which is of the utmost importance in the food industry.

Many investigations have focused on scraped surface heat exchangers (SSHE), studying their flow pattern characteristics [26], their thermo-hydraulic performance [10] or their scraping efficiency [25].

A series of works studied the performance of Newtonian and non-Newtonian flows inside scraped surface heat exchangers (SSHE) with rotating blades. Mabit et al. [19] used an electrodiffusion technique in order to investigate the shear rate on such devices, observing maximum shear rate at the scraping surface and on the leading edge of the blades. Yataghene et al. [31] undertook a numerical investigation to characterize the shear rates for Newtonian and Non-Newtonian fluids. Later, they [29] studied the effect of index and consistency behaviour of shear thinning fluid using power-law rheological behaviour on the viscous dissipation through a numerical model. Finally, they [30] performed an experimental analysis using Newtonian and non-Newtonian fluids where they studied flow patterns inside a scraped surface heat exchanger (SSHE) with a rotating blade under isothermal

* Corresponding author.
E-mail address: dcrespi@umh.es (D. Crespí-Llorens).

https://doi.org/10.1016/j.ijheatmasstransfer.2017.10.115
0017-9310/© 2017 Elsevier Ltd. All rights reserved.

Nomenclature

$a_i, \ldots, e_i$	correlation constants
D, R	inner diameter and radius of the pipe (Fig. 1)
d, R_s	diameter and radius of the insert device rod (Fig. 1)
D_h	hydraulic diameter, $D_h = D - d$
h_i	film coefficient inside the pipe
h	constant in function Δ
k	thermal conductivity
L_p	pressure ports separation length
m	flow consistency index (rheological property)
N	number of experimental measurements
Q	flow rate
P	distance from one scraper to the next one at the same angular position
Δp	pressure drop
r	radial position
t	scraper length (see Fig. 1)
T	temperature
U	uncertainty for a confidence level of 95%
u	fluid velocity
u_b	bulk velocity
v_s	velocity of the scraper (positive in co-current direction)

Greek symbols

γ	shear rate
μ_g	generalized viscosity of the flow, $\mu_g = m\,\phi(n)\left(\frac{u_b}{D_h}\right)^{n-1}$
ρ	fluid density
τ	shear stress

Dimensionless numbers

β	blockage parameter, $\beta = 1 - v_s/u_b$
Δ	relationship between axial velocity gradients at the heated wall, for a power law fluid and for a Newtonian fluid
f	Fanning friction factor, $f = \Delta p D_h / 2 L_p \rho u_b^2$
n	flow behaviour index (rheological property)
Nu	Nusselt number
Pr_g	generalized Prandtl number, $Pr_g = c_p \mu_g / k$
$Pr_{g,ref}$	reference Prandtl number for one set of experiments
$\phi(n)$	generalization function
Re_g	generalized Reynolds number, $Re_g = \rho u_b D_h / \mu_g$
ω	non-dimensional scraping velocity, $\omega = v_s/u_b = 1 - \beta$

Subscripts

a	the device under study (scraper)
av	section average value
g	non-dimensional number based on the generalized viscosity
sp	smooth pipe
dy, st	dynamic or static scraper respectively
w	value at the inner pipe wall

and continuous flow conditions. However, few studies have focused on the analysis of processes using non-Newtonian fluids within scraped surface heat exchangers (SSHE) with reciprocating scrapers, where the scraping device moves axially.

According to Chhabra and Richardson [7], pseudoplasticity is the most common non-Newtonian behaviour in the process industry. Pseudoplastic fluids are characterized by an apparent viscosity which decreases with increasing shear rate within a certain range of shear rates, and the Power Law model is widely used to represent this behaviour [13,6]. For such fluids, the friction factor depends on the Reynolds number and the pseudoplasticity of the fluid, represented in this model by the flow behaviour index n. Metzner and Reed [22] developed a generalization method for smooth pipes which defines a generalized fluid viscosity so that the friction factor depends only on the Reynolds number defined with such viscosity. Afterwards Kozicki et al. [18] and Delplace and Leuliet [11] extended its use to ducts with uniform cross section.

Recently, the authors [8] defined a generalized viscosity for geometries with non-uniform cross section in static conditions of the scraper and also studied the flow pattern in static and dynamic conditions [9]. In this research, the generalization method of the former work has been applied to the moving scraper. Experimental results will show the possibilities of applying this non-dimensional methodology, that simplifies and generalizes the study of the mechanical and thermal problems.

This work presents an experimental study of the heat transfer process to a pseudoplastic non-Newtonian fluid in a tubular SSHE. The scraper is shown in Fig. 1 and consists of semicircular shaped devices mounted on a moving rod. A hydraulic cylinder impels the whole alternatively along the axial direction and the device scrape the internal wall of the tube. The movement can be done sporadically to remove fouling, in that case, the study of the device in static conditions (static scraper) will be enough to evaluate its performance. In other cases, it will be better to actuate the scraper continuously at different velocities in order to increase heat transfer. In these situations, the power consumption of the movement has to be considered in the energy balance.

The research has two objectives. The first is to evaluate the performance of the device under study, which works with non-Newtonian fluids. For that, pressure drop, heat transfer and power consumption have been measured as functions of the involved variables: Reynolds number, Prandtl number and scraping velocity. The second objective is to evaluate the applicability of a generalization method for the viscosity of a power law fluid to the case of a moving scraping device.

Friction factor and Nusselt number have been correlated by employing the generalized viscosity on pressure drop and heat transfer results, both in static and dynamic conditions. Finally a performance evaluation of the heat transfer enhancement has been calculated to determine the negative effect of the power consumption for the scraping movement.

2. Experimental setup

The experimental set-up shown in Fig. 2(a) has been used to measure pressure drop, heat transfer and the moving rod power consumption for different flow regimes and scraping velocities.

2.1. Experimental set-up description

The experimental facility consists of two circuits:

- *The primary loop*, containing the test section (8) and the viscometer (12) in parallel.
- *The cooling loop*, which controls the temperature of the test fluid in the main tank(1).

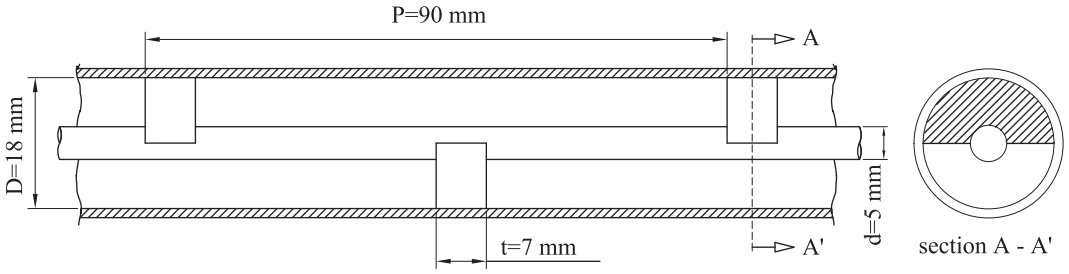

Fig. 1. Device under study.

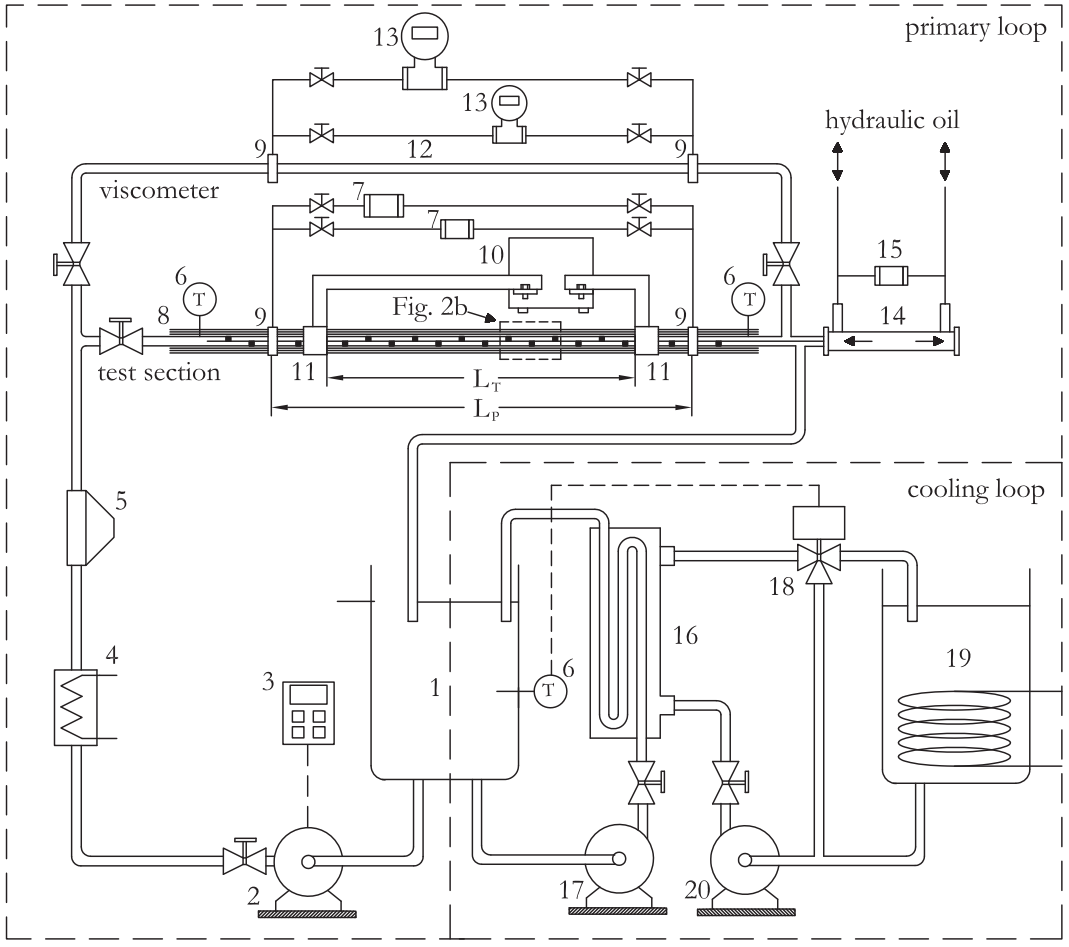

(a) Experimental set-up.

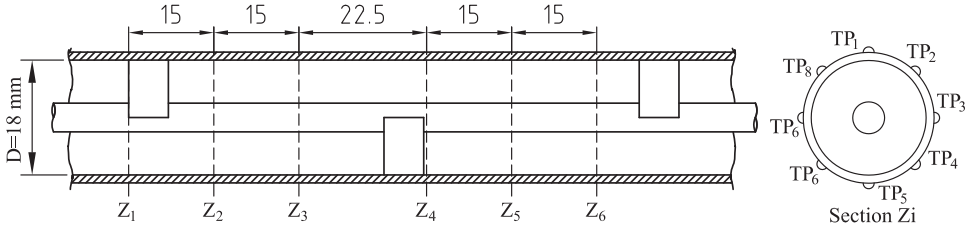

(b) Thermocouple distribution along the test section.

Fig. 2. Experimental set-up. (1) Test fluid tank, (2) primary loop gear pump, (3) frequency converter, (4) immersion resistance, (5) Coriolis flowmeter, (6) RTD temperature sensor, (7) non-stationary differential piezoresistive pressure transmitters, (8) stainless steel tube with an insert scraper and with inlet and outlet immersion RTDs, (9) pressure taps, (10) electric transformer, (11) electrodes, (12) smooth stainless steel pipe used as viscometer, (13) stationary pressure transmitters, (14) hydraulic piston, (15) non-stationary bidirectional differential piezoresistive pressure transmitter, (16) heat exchanger, (17) cooling loop gear pump, (18) three-way valve with a PID controller, (19) coolant liquid tank, (20) centrifugal pump.

The primary circuit can be manually configured to circulate the flow either through the test section or the viscometer.

The test section consists of a 4 m long, 2 mm thick, 18 mm internal diameter, 316L stainless steel tube with an insert device with the geometry shown in Fig. 1. A low-velocity gear pump (2) is used to circulate the working fluid. Such a type of pump has been selected to minimize fluid degradation during the experiments. A Coriolis flowmeter (5), which has been reported to perform properly when working with non-Newtonian fluids [12], measures mass flow rate and fluid density. The pressure drop is measured at pressure taps separated $L_p = 1.8$ m ($20P$). An entry region $L_e = 0.54$ m ($6P$) long, ensures fully developed periodic flow conditions. Each pressure connection (9) is composed of four boreholes separated 90°. Two non-stationary differential piezoresistive pressure transmitters Kistler 4264A (7) of ranges 0—2 bar and 0—5 bar have been used with this aim. The devices perform with an accuracy of 0.05% F.S.

The pressure drop of the fully developed stable flow within the viscometer is measured by means of two highly accurate stationary pressure transmitters SMAR LD301 (13) which are configured for different ranges.

With the aim of carrying out thermal experiments under uniform heat flux (UHF) conditions, two copper electrodes have been installed in the thermal test section, so that the heat is produced at the tube wall through the Joule effect. Power is supplied by a 6 kVA transformer (10), connected to a variable auto-transformer for power regulation. The distance between both electrodes is $L_T = 1.0$ m ($11P$). The total power transferred to the test section is obtained by measuring the voltage (0–15 V) and the electrical current (0–600 A). The pipe loop has been heavily insulated to minimize heat losses. The pipe outside wall temperature is measured by means of 48 K-type thermocouples distributed in six axial positions as shown in Fig. 2(b), where the first section is located a distance of 0.54 m ($6P$) downstream the first electrode. Fluid inlet and outlet temperatures are measured by two Resistance Temperature Detectors (RTDs) class B 1/10 DIN.

A hydraulic cylinder (14) propels the scraper in its axial movement. The pressure in the cylinder chambers is measured by a non-stationary bidirectional differential piezoresistive pressure transmitter of 0–20 bar (15), which allows us to determine the hydraulic system power consumption.

The test fluid temperature is controlled at the test fluid tank (1). Cooling is provided by the cooling loop (items 16–19) in Fig. 2(a)), which uses an oversize gear pump (17) to circulate the test fluid through a cooling heat exchanger (16). On the other side of the exchanger, the flow rate of the coolant fluid is controlled by a three-way-valve and a PID controller (18), which controls the temperature of the test fluid tank.

2.2. Test fluid characteristics

A 1 wt% aqueous solution of SigmaAldrich Co. carboxymethyl cellulose (CMC) has been used as test fluid. CMC powders with different chain length have been used.

The solutions have been prepared by dissolving the polymer powder in distilled water and then raising the pH values of the solution to increase viscosity. This fluid shows a non-Newtonian pseudoplastic behaviour which can be described by the *Power Law* model for a wide range of shear rates [1,13,2,28].

$$\tau = m\gamma^n \tag{1}$$

As per the studies of Chhabra and Richardson [7] and Cancela et al. [6], all CMC thermophysical properties except for the rheological parameters and fluid density have been assumed to be the same as pure water.

The type of CMC powder employed, the preparation method and fluid degradation due to shear stress and thermal treatment influence strongly the rheological fluid properties. This allows us to obtain fluids with different pseudoplastic behaviour, $m \in [4.6; 0.016]$ Pa s^n and $n \in [0.43; 1]$. The rheological properties of the non-Newtonian test fluid n and m are measured by the viscometer (item 10 in Fig. 2(a)). This procedure has been explained in detail previously [8]. The maximum uncertainty of the measurements of n and m are 0.01% and 0.4% respectively.

3. Experimental methodology

In order to simplify the analysis of the flow, a generalization method for the fluid viscosity has been used, which provides an expression for the parameter $\phi(n)$ in Eq. (2). The resulting generalized viscosity is used for the definition of the Reynolds and Prandtl numbers, Re_g and Pr_g.

$$\mu_g = m\,\phi(n)\left(\frac{u_b}{D_h}\right)^{n-1} \tag{2}$$

The definition of $\phi(n)$ for the geometry under study (Fig. 1) was provided by Crespí-Llorens et al. [8] for static conditions of the scraper,

$$\phi(n) = 262.27^{n-1}n^{-2.1177} \tag{3}$$

Besides, in Section 6, the definition of $\phi(n)$ by Metzner [21] is used for the smooth pipe geometry.

A correction factor for non-Newtonian fluids has been applied to obtain correlations free from variable property effects [17,16].

$$Nu = \frac{h_i D_h}{k}\left(\frac{m_{av}}{m_w}\right)^{0.44n-0.58} \tag{4}$$

Besides, in order to simplify the study, a parameter $\Delta^{1/9}$ is used to account for the influence of the non-Newtonian behaviour in the Nusselt number [14,20].

$$\Delta = \frac{\left(\frac{\partial u}{\partial r}\Big|_{r=R}\right)_{n\neq 1}}{\left(\frac{\partial u}{\partial r}\Big|_{r=R}\right)_{n=1}} = \frac{24n+h}{(24+h)n} \tag{5}$$

In this work, the value of $h = 7.532$ is used for the annulus geometry, which has been obtained by means of the numerical model described previously by the authors [9].

For both pressure drop and heat transfer measurements, the experiments in both static and dynamic conditions have been carried out in sets and the rheological properties have been measured at the beginning and the end of each set.

In Section 6.1, the performance of the device is compared to the performance of pure forced convection inside a smooth pipe. The behaviour of non-Newtonian fluids in the reference geometry has been obtained by a numerical model.

The uncertainties have been calculated according the "Guide to the expression of uncertainty in measurement", published by the ISO [15]. The uncertainty of Re_g and Pr_g depend strongly on the uncertainty of the experimental generalization method, being 11% for both parameters. The uncertainty of the Fanning friction factor f and the Nusselt number Nu are 1% and 2%, respectively.

4. Pressure drop results in dynamic conditions

For experiments in dynamic conditions, the scraper moves continuously in co-current and counter-current directions. A full cycle is defined as the time taken by the scraper to make its co-current movement and its counter-current one. Both half cycles have been

studied separately in Section 4.1 and the average pressure drop of the full cycle is studied in Section 4.2.

4.1. Pressure drop in co-current half cycle and in counter-current half cycle

In this section, pressure drop has been measured in the co-current and the counter-current movements of the scraper separately. Previous visualization studies [9], have found the structure of the flow to be strongly dependent on the blockage of the flow, defined as follows:

$$\beta = 1 - v_s/u_b \tag{6}$$

In particular three different structures were identified for the following values: $\beta > 0, \beta = 0$ and $\beta < 0$. The flow velocity pattern for $\beta = 0$ is intermediate between the other two, being almost equal to the flow in annulus geometry. Being the case of the static scraper ($\beta = 1$) a case of positive blockage, the flow structure is similar to other cases with $\beta > 0$. From Eq. (6), these cases occur for $v_s < u_b$, and thus, for low scraping velocities in both directions or counter-current direction in any case.

A total of 450 experiments have been carried out for $Re_g \in [1; 200]$ and $\beta \in [0.2; 2.5]$. The rheological properties of the different fluids which have been used in the experiments are within the ranges $n \in [0.43; 1]$ and $m \in [4.26; 0.016]$ Pa s^n.

As stated before, the two different half cycles of the scraping movement (each with a different value of β) have been studied separately. On the one hand, pressure drop results in the co-current direction of the scraping movement are shown in Fig. 3 for experiments with $\beta = 0.5, 0.7, 0.8, 0.9$. For the experiments with $\beta = 0.9$, the flow is laminar up to $Re_g \approx 110$, where the transition occurs. For the experiments with a lower value of β, the transition region is not observed that clearly, due to the lack of results for high Reynolds numbers. On the other hand, pressure drop results in the counter current direction are shown in Fig. 4 for experiments with $\beta = 1.1, 1.2, 1.3, 1.5, 2, 2.5$. As it can be appreciated, for higher values of β, the transition is reached at lower Reynolds numbers. However, for the experiments with higher β, the transition is not reached due to experimental limitations.

The results in the laminar region have been correlated with Eq. (7) for co-current and counter-current scraping directions. The values for the constants of the equations for both cases are detailed in Table 1(a) and the correlation is shown in Figs. 3 and 4.

$$f = a_1 Re_g^{b_1} \beta^{c_1} \tag{7}$$

In both scraping directions, the results show the expected increase in pressure drop as the *blockage of the flow*, β, increases.

Besides, the assumption of the validity of the generalization method for the cases with $\beta > 0$ has been confirmed, as the friction factor f in experiments with different fluid characteristics has been found to follow the same correlation with Re_g.

4.2. Full cycle average pressure drop

In standard operation conditions, the scraper works in full cycles with a constant value of $|v_s|$, being v_s negative for the counter-current half-cycle and positive for the co-current one. Consequently, the study of the average pressure drop for the full

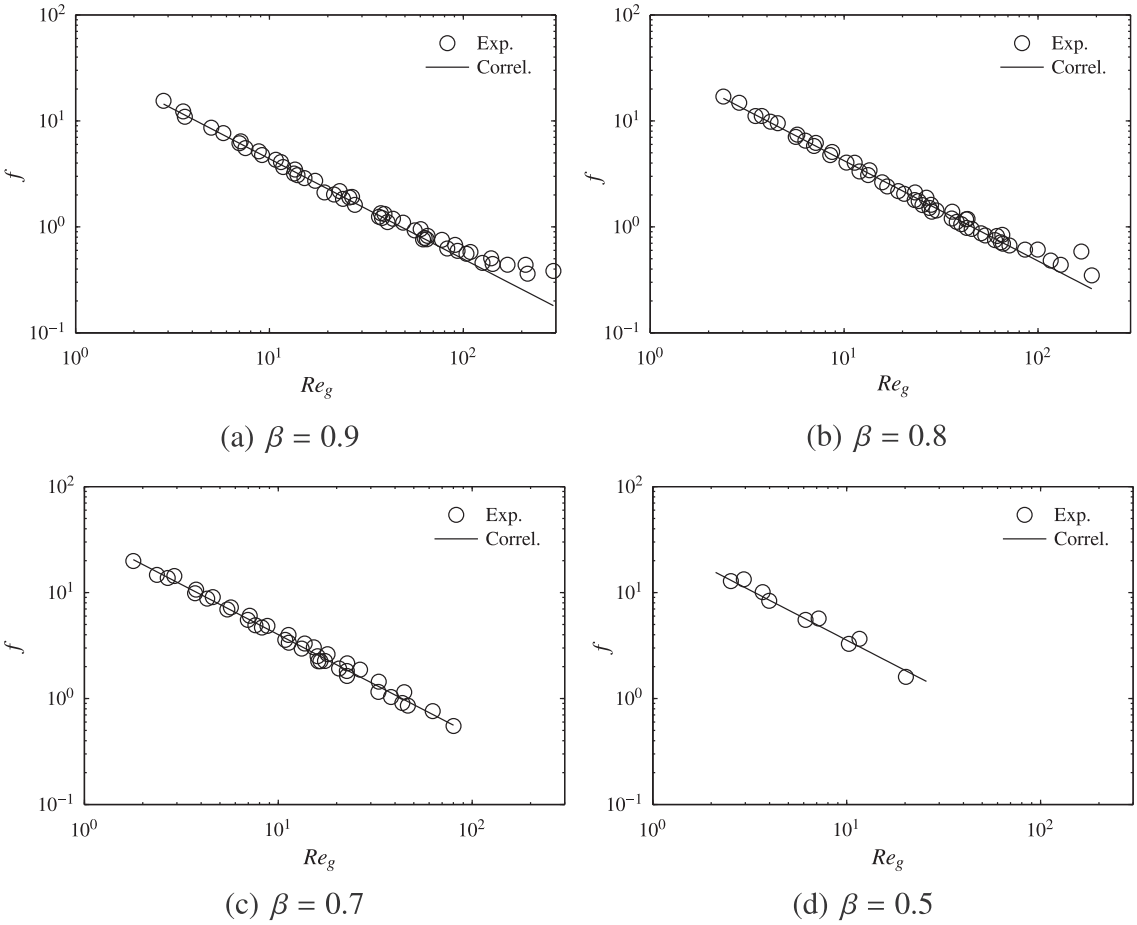

Fig. 3. Experimental pressure drop measurements and correlation during the co-current movement of the scraper. Correlation according to Eq. (7 and Table 1(a).

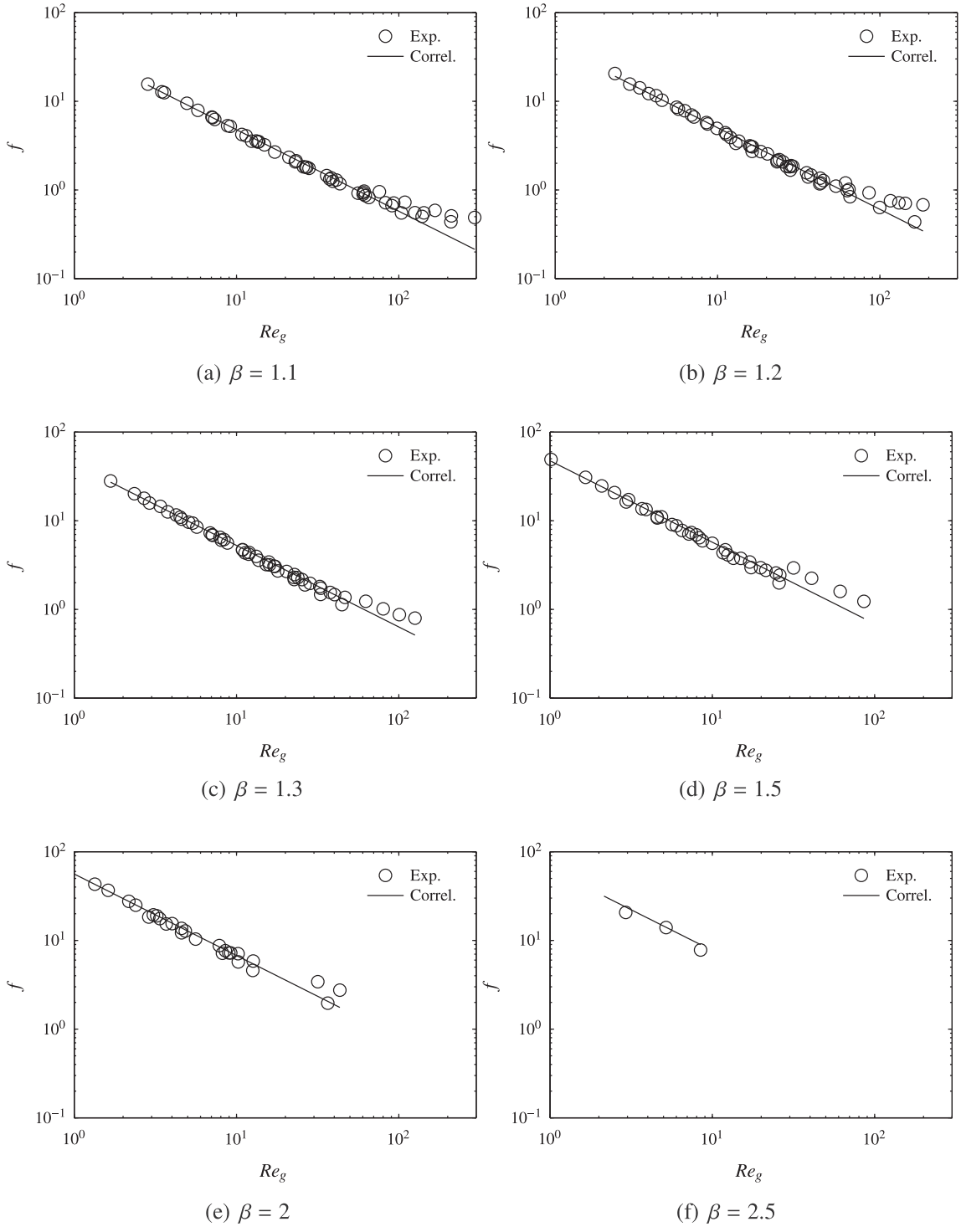

Fig. 4. Experimental pressure drop measurements and correlation during the counter-current movement of the scraper. Experimental correlation according to Eq. (7) and Table 1(a).

cycle of the scraper movement has been found of interest. In this case, the non-dimensional scraping velocity will be used for the analysis:

$$\omega = v_s/u_b \tag{8}$$

Experiments have been carried out at Reynolds numbers within the range $Re_g \in [1; 200]$, at different scraping velocities $|\omega| = 0.1; 0.2; 0.3; 0.5$, being the rheological properties of the fluid within the ranges $n \in [0.45; 1]$ and $m \in [4.53; 0.1]$ Pa s^n.

The results in Fig. 5 show that, within the analysed range, the impact of the scraping velocity on the average pressure drop in the laminar region is not significant. Therefore, the experiments have been correlated (Table 1(b)) to

$$f = a_2 Re_g^{b_2} \tag{9}$$

For experiments with higher non-dimensional scraping velocity ω, the transition is observed to occur for lower Reynolds numbers. Besides, for high Reynolds numbers, experiments with higher ω show higher pressure drop.

Table 1
Pressure drop experimental correlation constants in dynamic conditions. Laminar flow.

	Co-current	Counter-current
(a) Pressure drop on each scraping half-cycle (Eq. (7))		
a_1	44.93	40.63
b_1	−0.9593	−0.9307
c_1	0.4624	0.54
$U(f)$	15.4%	14.2%

a_2	b_2	$U(f)$
(b) Full-cycle average pressure drop (Eq. (9))		
39.52	−0.9558	14.6%

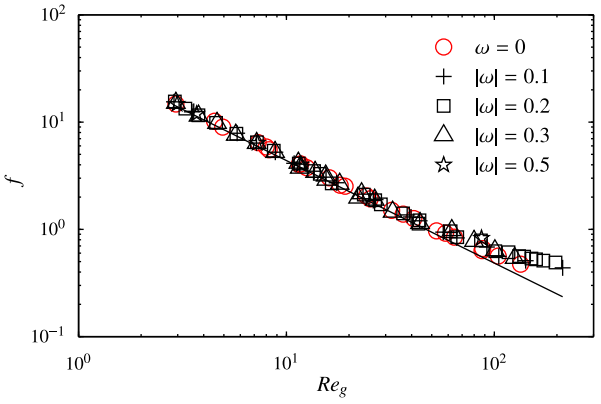

Fig. 5. Full cycle average pressure drop and experimental correlations for the laminar flow region (Table 1(b)).

The results of the experiments with the static scraper within the same range of Reynolds numbers has been plotted in Fig. 5 as well. The data shows that, in the laminar flow region, there is no significant difference between the pressure drop in static and dynamic conditions of the scraper within the analysed ranges.

5. Heat transfer results

Heat transfer to pseudoplastic non-Newtonian fluids has been analysed in static and dynamic conditions of the scraper.

5.1. Heat transfer in static conditions

Pseudoplastic fluids with rheological properties in the ranges $n \in [0.45; 0.94]$ and $m \in [4.6; 0.04]$ Pa.s^n have been used as test fluid for heat transfer experiments in static conditions of the scraper. A total of 120 experiments, grouped in 11 sets, have been carried out within the following ranges of Reynolds and Prandtl numbers: $Re_g \in [0.4; 320]$ and $Pr_g \in [180; 4500]$. The properties of the experiments within a set are detailed in Table 2(a).

For the results, four regions of the fluid have been identified:

- *Region I.* Laminar attached flow.
- *Region II.* Laminar detached flow.
- *Region III.* Transition from laminar to turbulent flow.
- *Region IV.* Turbulent flow.

The obtained results have been correlated to Eq. (10), where the Δ parameter has been defined in Section 2.

$$Nu = a_3 Re_g^{b_3} Pr_g^{c_3} \Delta^{1/9} \tag{10}$$

On the one hand, the correlation constants are shown in Table 3 (b) for all the regions of the fluid but the transition one. On the other hand, the fluid regions are shown in Fig. 6, where, for a better understanding, the results for all the experiments have been transported to $Pr_g = 1000$, by using Eq. (10).

By using a non-Newtonian highly viscous fluid, valuable data have been obtained for very low Reynolds. This has permitted us to identify two different laminar regions (I and II). Region I is defined for $Re_g < 4$, while region II is defined for $4 < Re_g < 30$. In region I, the boundary layer is attached to the boundary solids, while in region II there is a boundary layer detachment downstream each semicircular piece, but the flow remains laminar [9].

As it can be observed in Fig. 6, the Nusselt number dependence on the Reynolds number is lower in region I than in region II. This is due to the differences in the flow pattern in regions I and II. The more important is the boundary layer detachment after the semicircular pieces, the higher the heat transfer enhancement. It is noteworthy that no differences have been found between regions I and II in pressure drop results.

The transition to the turbulent flow begins at $Re_g \approx 30$ and the flow is fully turbulent (region IV) for $Re_g > 65$. In region III (transitional flow), the Nusselt number has a low dependence on the Reynolds number and higher dependence on the Prandtl number, but

Table 2
Static conditions heat transfer experiments.

Exp	T (°C)	n	m (Pa s^n)	Pr_g	$Pr_{g,ref}$
(a) Experiment sets characteristics					
HT1	20	0.85—0.82	0.1091—0.2297	415—550	500
HT2	18	0.86—0.84	0.1244—0.1836	394—529	470
HT3	35	0.79—0.8	0.2216—0.1838	307—481	390
HT4	35	0.93—0.94	0.0488—0.0433	180—201	190
HT5	15	0.45—0.45	4.571—4.527	1240—4500	2960
HT6	25	0.46—0.47	3.873—3.470	967—4240	2400
HT7	35	0.52—0.52	2.113—2.093	637—2560	1430
HT8	15	0.60—0.60	1.439—1.371	712—2110	1320
HT9	25	0.62—0.64	1.026—0.886	556—1510	940
HT10	35	0.69—0.70	0.5510—0.4820	413—865	630
HT11	25	0.74—0.74	0.3810—0.3622	396—721	550

Flow region	a_3	b_3	c_3	$U(Nu)$
(b) Correlation constants (Eq. (10))				
I	0.4037	0.3735	0.3002	4.8%
II	0.4148	0.5921	0.2352	7.4%
IV	0.0259	1.1107	0.2354	19.8%

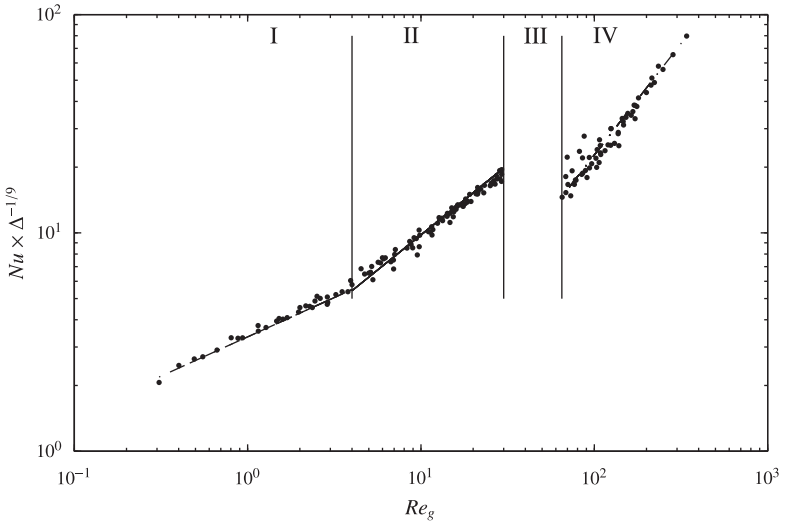

Fig. 6. Flow regions. All the experiment results have been transported to $Pr_g = 1000$ by using Eq. (10). Results at region III cannot be transported.

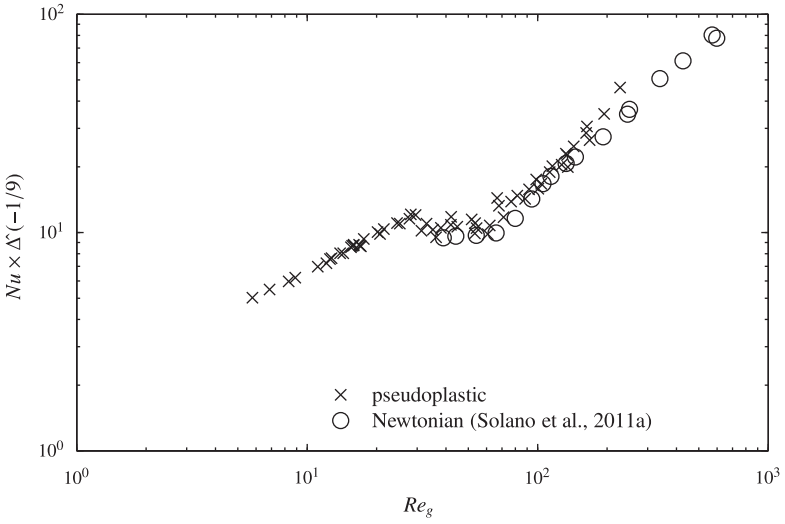

Fig. 7. Validation of the heat transfer results in static conditions of the scraper by comparison with equivalent results with Newtonian flows at $Pr_g = 300$. The results correspond to experiment sets HT1, HT2, HT3 and HT11.

no correlation can be obtained for this region, due to the high variability of the results.

The validation of the results in Fig. 7 has been carried out by comparing them to the ones obtained by Solano et al. [23] for Newtonian fluids inside the same device for Prandtl numbers $Pr = Pr_g = 300$. The comparison is shown in Fig. 7. Despite de difference in the viscosity of the fluids, the results overlap in region III and part of region IV, showing a good matching.

5.2. Heat transfer in dynamic conditions

In dynamic conditions of the scraper, a total of 197 experiments in 9 sets (Table 3(a)) have been carried out at low scraping velocities $|\omega| \in [0.1; 1]$ within the following ranges: $Re_g \in [1.3; 216]$ and $Pr_g \in [215; 2600]$. For that, pseudoplastic test fluids with rheological properties within the ranges $n \in [0.45; 0.94]$ and $m \in [4.6; 0.04]$ Pa.s^n have been used.

As in Section 5.1, four flow regions have been identified with equivalent characteristics. The results in regions I, II and IV have been correlated to Eq. (11) and the constants results are shown in Table 3(b). The average value of Δ in both scraping cycles for an annulus geometry is practically equal to the one of the static case, so the latter has been used.

$$Nu = a_4 Re_g^{b_4} Pr_g^{c_4} (d_4 + |\omega|)^{e_4} \Delta^{1/9} \tag{11}$$

The values of the correlation constants in Table 3(b) show that the influence of the Reynolds number and Prandtl numbers are similar to the ones in the static case, while the movement of the scraper produces heat transfer enhancement in all fluid regions. In order to observe the latter, heat transfer results for different scraping velocities (including the static case for $\omega = 0$) are shown in Fig. 8. The figure shows as well that the transitional flow region is smaller, the greater the scraping velocity.

The validation step is carried out again by comparing results to the existing ones for Newtonian fluids [24] for similar Prandtl numbers. Such comparison is shown in Fig. 9. Once again, the influence of the non-Newtonian fluid behaviour is characterized by the definitions of the generalized viscosity μ_g and the parameter Δ.

Table 3
Dynamic conditions heat transfer experiments.

Exp	T (°C)	n	m (Pa s^n)	Pr_g
(a) Dynamic conditions heat transfer experiments				
DHT-1	16.17–17.23	0.48–0.53	2.862–1.928	215–2120
DHT-2	16.9–17.61	0.59–0.63	1.292–0.8988	632–1450
DHT-3	16.7–16.3	0.81–0.82	0.2235–0.1907	410–600
DHT-4	17.2–18	0.93–0.94	0.0624–0.0551	250–290
DHT-5	25.8–25.5	0.75–0.74	0.3478–0.3588	456–746
DHT-6	16.9–16	0.69–0.71	0.6303–0.5910	630–1070
DHT-7	17.6–17.0	0.52–0.52	2.640–2.557	790–2625
DHT-8	18.0–17.7	0.62–0.64	1.164–0.9691	700–1590
DHT-9	15.8–15.8	0.87–0.89	0.1267–0.1118	330–425

Region	Re_g	a_4	b_4	c_4	d_4	e_4	N	$U(Nu)$
(b) Correlation constants (Eq. (11))								
I	1 – 4	0.0212	0.6677	0.6102	1.2401	1.5544	26	15.1%
II	4 – 30	0.2584	0.5989	0.3702	0.6511	0.9300	147	6.6%
IV	> 50	0.0566	0.8977	0.3820	2.2×10^{-10}	0.0179	24	21.7%

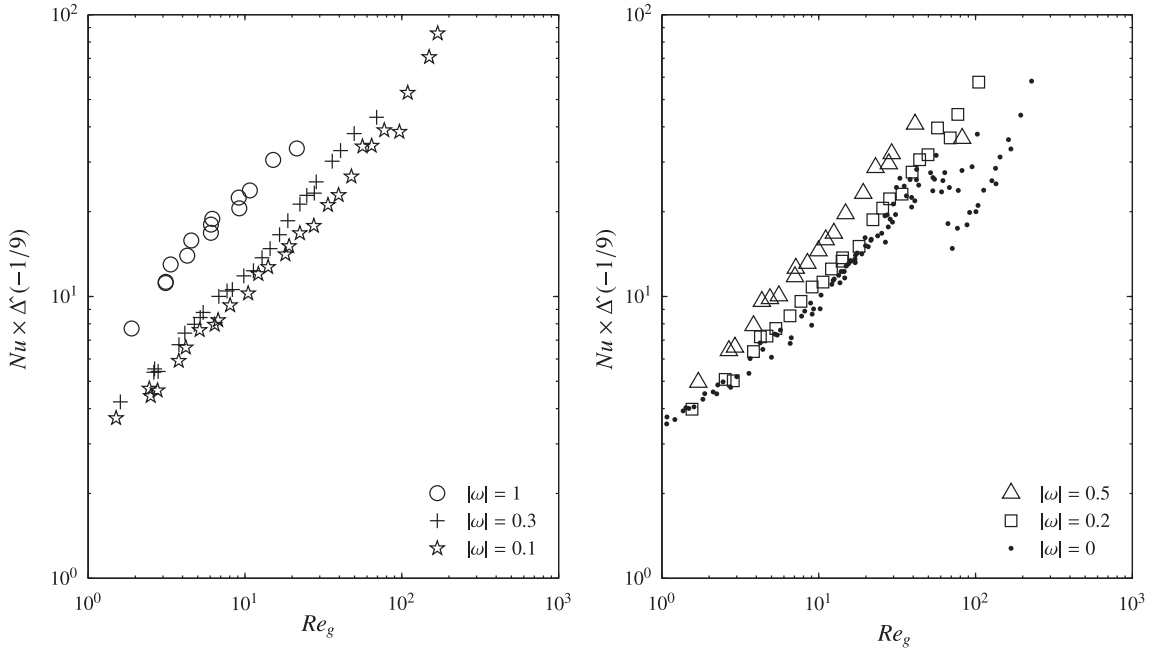

Fig. 8. Scraping velocity effect on the Nusselt Number. Experimental data has been transported to $Pr_g = 1000$.

Besides, Figs. 7 and 9 show the different working ranges of Reynolds numbers for Newtonian and non-Newtonian fluids. Although the viscosity depends on the working fluid and the working conditions, the compared cases are very representative of the fluids in the process industry, as non-Newtonian fluids are usually significantly more viscous than Newtonian fluids.

6. Performance evaluation of the device

The overall performance of the device has been evaluated in static and dynamic conditions of the scraper. To that end, two classic criteria defined by Bergles et al. [3] and Webb [27] have been used:

- R1 criterion: Shows the heat transfer enhancement for the same flow rate and exchange area ($Q_a/Q_{sp} = 1, \dot{A}_a/\dot{A}_{sp} = 1$).
- R3 criterion: Shows the heat transfer enhancement for the same power consumption and exchange area ($\dot{W}_a/\dot{W}_{sp} = 1$, $\dot{A}_a/\dot{A}_{sp} = 1$). In this criterion, the consumption of the circulating pump and the rod propelling system (in dynamic conditions of the scraper) have been considered.

6.1. Performance evaluation in static conditions

The performance of the device under study has been compared to a *smooth pipe* of the same length and with a diameter equal to the hydraulic diameter of the device under study (D_h). However, it should be taken into account, that in the applications for which the current device is intended, a simple pipe heat exchanger is not an option, due to the strong fouling formation.

The comparison has been carried out by using both the R1 and the R3 criteria. Both R1 and R3 criteria are formulated as a Nusselt number ratio.

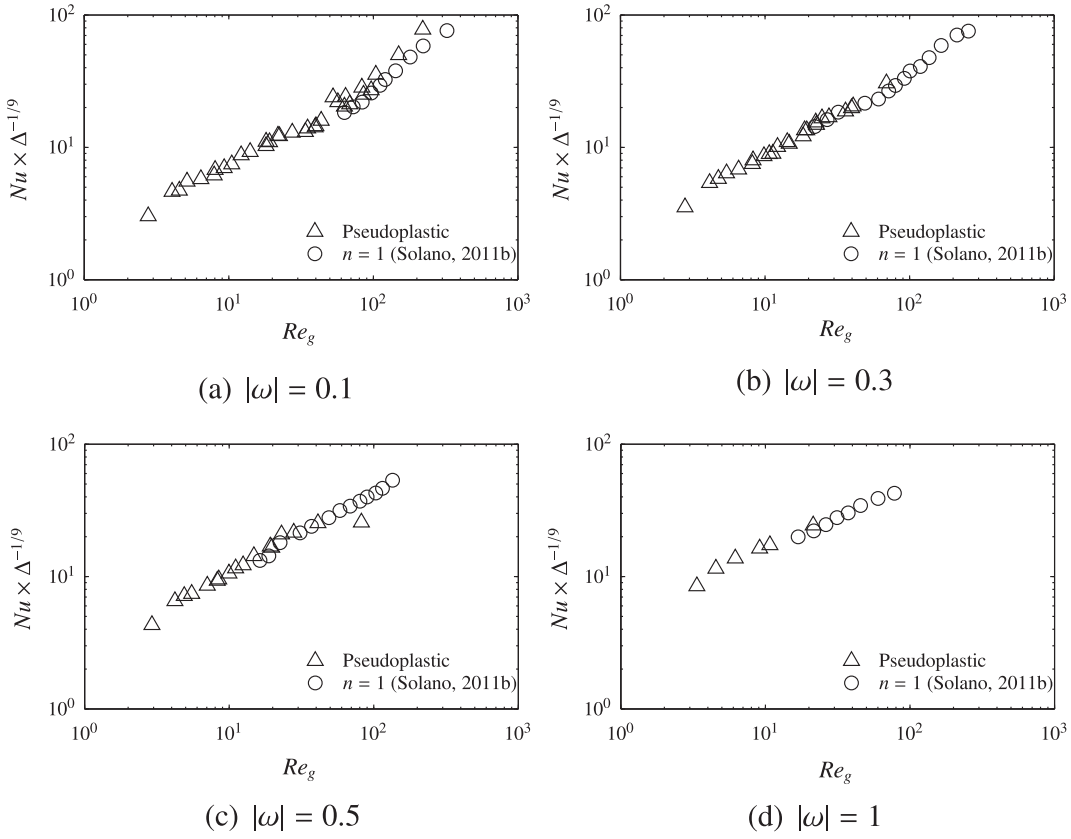

Fig. 9. Comparison of Nusselt number results working with pseudoplastic (transported to $Pr_g = 450$) and Newtonian fluids ($Pr = 450$).

The R1 criterion compares situations which comply with the following relation between Reynolds numbers

$$\frac{Re_{g,sp}}{Re_{g,a}} = \frac{\phi_a(n)}{\phi_{sp}(n)} \left(\frac{D+d}{D_h}\right)^{2-n} \tag{12}$$

and the R3 criterion compares situations which comply with

$$\frac{Re_{g,sp}}{Re_{g,a}} = \frac{\phi_a(n)}{\phi_{sp}(n)} \left[\frac{f_a}{f_s p}\left(1+\frac{d}{D}\right)\right]^{(2-n)/3} \tag{13}$$

The R1 criterion in Fig. 10 shows heat transfer enhancements for the scraper for $Re_{g,a} > 20$ which approximately corresponds to the beginning of region III, being very significant for turbulent flow regimes (region IV, $Re_{g,a} > 65$), where heat transfer has increased

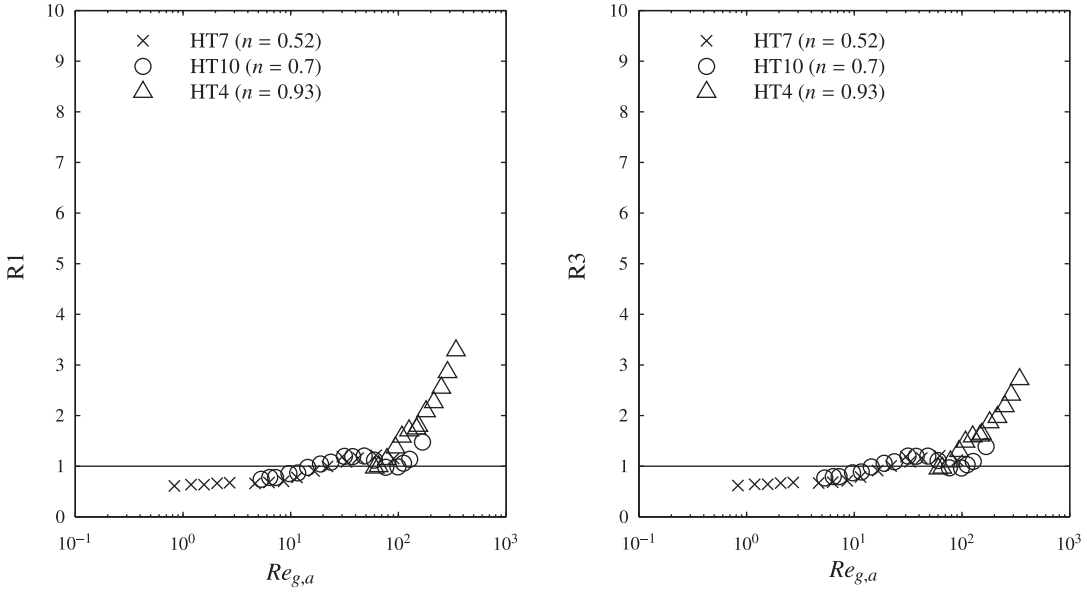

Fig. 10. Performance evaluation of the scraper in static conditions. Static scraper vs. pure forced convection in a smooth pipe.

up to more than 3 times. The main reason for this enhancement is that the presence of the semicircular plugs causes the transition to turbulent flow to take place for much lower Reynolds numbers than in the smooth pipe. However, for low Reynolds numbers ($Re_{g,a} < 20$) the scraper lessens heat transfer. This is due to the presence of the plastic semicircular plugs which have poor heat conductivity.

The R3 comparison shows similar results to the R1 comparison. However, as the scraper increases pumping requirements, the R3 shows lower heat transfer enhancement than the R1 criterion (up to 2.8 times versus up to 3.4 times).

6.2. Performance evaluation of the scraping movement

In this section, the performance of the device under dynamic conditions of the scraper has been evaluated. To that end, its performance in dynamic conditions has been compared to its performance in static conditions. This way, the choices of continuously actuating the scraper at different velocities or only sporadically to remove fouling, have been evaluated.

Firstly, the R1 criterion is plotted in Fig. 11. The results show that actuating the insert device enhances heat transfer in any case. Besides, the faster the insert device moves alternately, the greater heat transfer enhancement is obtained within the studied range of scraping velocities ($|\omega| \in [0.1; 1]$). Heat transfer enhancements in the laminar flow regions (referring to the case of the static scraper) can be up to 1.2 times for a scraping velocity of $|\omega| = 0.2$, up to 1.7 times for $|\omega| = 0.5$ and up to 2.5 times for $|\omega| = 1$. Furthermore, for the turbulent flow region (referred to the case of the static device), heat transfer enhancements are far greater, reaching values of 1.8 times for $|\omega| = 0.2$ and 2.4 times for $|\omega| = 0.5$. Nonetheless, only a few values have been obtained for this region, due to the high viscosity of the test fluid.

Secondly, the R3 criterion has been plotted in Fig. 12 for sets of experiments with different fluid rheology. This criterion takes into account the energy consumption of both the pumping system and the propelling system for the rod, by comparing situations with the same energy consumption. The results show that, as a general rule for the experiments which have been carried out, for $Re_{g,dy} < 50$, and without taking fouling into account, it is energetically not interesting to continuously actuate the device. However, for the experiments with higher Reynolds numbers, it will be energetically interesting to actuate the scraping device at low scraping velocities in order to minimize power consumption. For the fluid with the strongest pseudoplastic behaviour (DHT-1, $n \approx 0.5$), $R3 > 1$ for about $Re_{g,dy} > 50$, while for the almost Newtonian fluid (DHT-4, $n \approx 0.93$), $R3 > 1$ for about $Re_{g,dy} > 120$. From this, it can be concluded that the limiting Reynolds number for the R3 criterion decreases with the pseudoplasticity of the fluid.

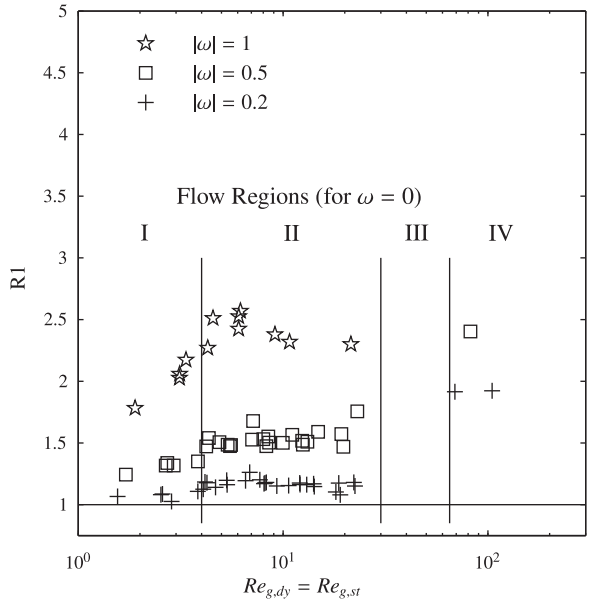

Fig. 11. Performance evaluation of the scraper movement by using the R1 criterion. Dynamic vs. static conditions.

7. Conclusions

After analysing the obtained results as a whole, it can be concluded that the scraper is suitable to work with non-Newtonian fluids. However, the recommended working ranges depend on many factors which shall be studied for each case individually. Working in static conditions is energetically the most efficient solution, however, to avoid or prevent fouling, some scraping movement will be required sporadically or continuously.

The movement of the insert device has been proved to produce heat transfer increase in any situation which has been studied, although significantly increasing power consumption. The foregoing can be useful to control very precisely heat transfer in an industrial process. Furthermore, some products, especially in the food industry, need to be at a quite uniform temperature: if the product reaches too high temperatures near the wall, its quality will decrease significantly and can even boost fouling formation.

The main conclusions of this research are summarized next:

- Pressure drop, heat transfer and power consumption measurements, using non-Newtonian pseudoplastic fluids, have been carried out in static and dynamic conditions of the scraper.
- Four flow regions have been identified: attached laminar, detached laminar, transitional and turbulent flow regions.
- A generalization method for the fluid viscosity, that includes the effects of the non-Newtonian fluid behaviour, has been used.
- The friction factor and the Nusselt number have been successfully correlated by employing the generalized viscosity on pressure drop and heat transfer results, both in static and dynamic conditions and for three of the four identified flow regions (it was not possible to get correlations in the transitional region).
  - The friction factor depends on the generalized Reynolds number and on the blockage of the flow.
  - The Nusselt number in static and dynamic conditions has been found to depend on the generalized Reynolds number, the generalized Prandtl number, the non-dimensional scraping velocity and the non-Newtonian behaviour of the flow.
- Under no-fouling conditions, the device in static conditions is found to perform better than a smooth pipe heat exchanger for Reynolds numbers over 10, reaching significant heat transfer enhancements if the turbulent region is reached. Furthermore, actuating the scraper increases heat transfer in any case, but also increases energy consumption.
- The device is suitable for an industrial process using non-Newtonian fluids, since it prevents fouling, increases heat transfer, provides flexibility and enhances the final product quality. Furthermore, the obtained correlations are a valuable tool in the design of heat exchangers.

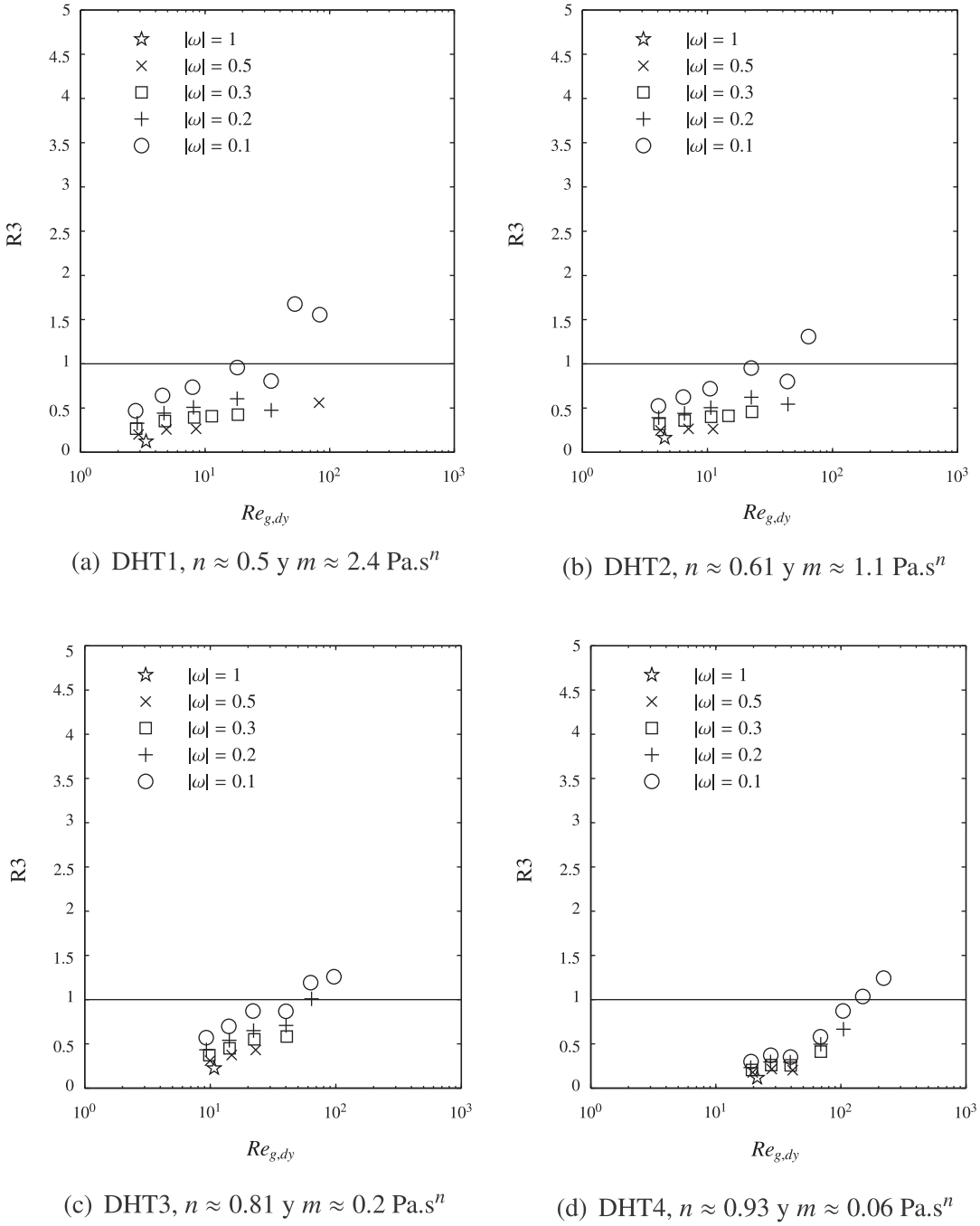

(a) DHT1, $n \approx 0.5$ y $m \approx 2.4$ Pa.s^n

(b) DHT2, $n \approx 0.61$ y $m \approx 1.1$ Pa.s^n

(c) DHT3, $n \approx 0.81$ y $m \approx 0.2$ Pa.s^n

(d) DHT4, $n \approx 0.93$ y $m \approx 0.06$ Pa.s^n

Fig. 12. Dynamic vs. static scraper. R3 criterion. At the *x*-axis, $Re_{g,dy}$ corresponding to dynamic experiments is plotted.

Conflicts of interest

None.

Acknowledgements

This work was supported by the Ministry of Education of the Spanish Government [AP2007-03429], which covered the expenses of a 4-year research at *Universidad Politécnica de Cartagena*, as well as a stage at the University of Sheerbroke in Canada, where part of this research was carried out. It was further covered by the Ministry of Science and Innovation (DPI2007-66551-C02-01).

Appendix A. Supplementary material

Supplementary data associated with this article can be found, in the online version, at https://doi.org/10.1016/j.ijheatmasstransfer.2017.10.115.

References

[1] K.A. Abdelrahim, H.S. Ramaswamy, High temperature/pressure rheology of carboxymethyl cellulose (CMC), Food Res. Int. 28 (1995) 285–290, https://doi.org/10.1016/0963-9969(94)00045-A. <http://www.sciencedirect.com/science/article/B6T6V-3YGV363-1X/2/684a277b59f1fb8440f6843c4d573075>.

[2] B. Abu-Jdayil, Modelling the time-dependent rheological behavior of semisolid foodstuffs, J. Food Eng. 57 (2003) 97–102, https://doi.org/10.1016/S0260-8774(02)00277-7. <http://www.sciencedirect.com/science/article/B6T8J-474GHDY-1/2/aec185ebbc6f352b06ad4363ece2fb8f> .
[3] A. Bergles, A.R. Blumenkrantz, J. Taborek, Performance evaluation criteria for enhanced heat transfer surface, J. Heat Transfer 2 (1974) 239–243.
[4] M. Beuf, G. Rizzo, J. Leuliet, H. Müller-Steinhagen, A. Karabelas, S. Yiantsios, T. Benezech, Fouling and cleaning of modified stainless steel plate heat exchangers processing milk products, in: Heat Exchanger Fouling and Cleaning: Fundamentals and Applications, 2003.
[5] W. Blel, P. Legentilhomme, T. Bénézech, F. Fayolle, Cleanability study of a scraped surface heat exchanger, Food Bioprod. Process. 91 (2013) 95–102, https://doi.org/10.1016/j.fbp.2012.10.002. <http://www.sciencedirect.com/science/article/pii/S0960308512000909> .
[6] M. Cancela, E. Alvarez, R. Maceiras, Effects of temperature and concentration on carboxymethylcellulose with sucrose rheology, J. Food Eng. 71 (2005) 419–424, https://doi.org/10.1016/j.jfoodend.2004.10.043. <http://doi.wiley.com/10.1016/j.jfoodend.2004.10.043> .
[7] R. Chhabra, J. Richardson, Non-Newtonian Flow and Applied Rheology. Engineering Applications, Butterworth-Heinemann, 225 Wildwood Av., Woburn, 2008.
[8] D. Crespí-Llorens, P. Vicente, A. Viedma, Generalized Reynolds number and viscosity definitions for non-Newtonian fluid flow in ducts of non-uniform cross-section, Exp. Therm. Fluid Sci. 64 (2015) 125–133. <https://doi.org/10.1016/j.expthermflusci.2015.02.005> .
[9] D. Crespí-Llorens, P. Vicente, A. Viedma, Flow pattern of non-Newtonian fluids in reciprocating scraped surface heat exchangers, Exp. Therm. Fluid Sci. 76 (2016) 306–323, https://doi.org/10.1016/j.expthermflusci.2016.03.002. <http://www.sciencedirect.com/science/article/pii/S0894177716300401> .
[10] R. De Goede, E. De Jong, Heat transfer properties of a scraped-surface heat exchanger in the turbulent flow regime, Chem. Eng. Sci. 48 (1993) 1393–1404.
[11] F. Delplace, J. Leuliet, Generalized Reynolds number for the flow of power law fluids in cylindrical ducts of arbitrary cross-section, Chem. Eng. J. Biochem. Eng. J. 56 (1995) 33–37, https://doi.org/10.1016/0923-0467(94)02849-6. <http://www.sciencedirect.com/science/article/B6V5M-3YYTDSS-5/2/e9b148aadd392be7faef790e07cb761> .
[12] I. Fyrippi, I. Owen, M. Escudier, Flowmetering of non-Newtonian liquids, Flow Meas. Instrum. 15 (2004) 131–138.
[13] M.T. Ghannam, M.N. Esmail, Rheological properties of carboxymethyl cellulose, J. Appl. Polym. Sci. 64 (1996) 289–301, https://doi.org/10.1002/(SICI)1097-4628(19970411)64:2<289::AID-APP9>3.0.CO;2-N. <http://doi.wiley.com/10.1002/(SICI)1097-4628(19970411)64:2<289::AID-APP9>3.0.CO;2-N> .
[14] U. Grigull, Wärmeübergang an nicht-newtonsche flüssigkeiten bei laminarer rohrströmung, Chem. Ing. Tech. 28 (1956) 553–556, https://doi.org/10.1002/cite.330280808. <https://doi.org/10.1002/cite.330280808> .
[15] ISO, 1995. Guide to the Expression for Uncertainty Measurement, first ed., International Organization for Standardization, Switzerland.
[16] S. Joshi, A. Bergles, Experimental study of laminar heat transfer to in-tube flow of non-Newtonian fluids, J. Heat Transfer 102 (1980) 397–401.
[17] S.D. Joshi, Heat Transfer in in-tube Flow of Non-Newtonian Fluids (Ph.D. Thesis), Iowa State University, Ames, Iowa, 1978.
[18] W. Kozicki, C.H. Chou, C. Tiu, Non-Newtonian flow in ducts of arbitrary cross-sectional shape, Chem. Eng. Sci. 21 (1966) 665–679, https://doi.org/10.1016/0009-2509(66)80016-7. <http://www.sciencedirect.com/science/article/B6TFK-4435YC2-8K/2/a1a87db5072fe58e9a3796572d72ea77> .
[19] J. Mabit, F. Fayolle, J. Legrand, Shear rates investigation in a scraped surface heat exchanger, Chem. Eng. Sci. 58 (2003) 4667–4679, https://doi.org/10.1016/j.ces.2003.07.001. <http://www.sciencedirect.com/science/article/pii/S0009250903003373> .
[20] D. Martínez, A. García, J. Solano, A. Viedma, Heat transfer enhancement of laminar and transitional Newtonian and non-Newtonian flows in tubes with wire coil inserts, Int. J. Heat Mass Transfer 76 (2014) 540–548.
[21] A. Metzner, Heat transfer in non-Newtonian fluids, in: J. Hartnett, J.T.F. Irvine (Eds.), Advances in Heat Transfer, vol. 2, Academic Press, New York, 1965, pp. 357–397.
[22] A.B. Metzner, J.C. Reed, Flow of non-Newtonian fluids – correlation of the laminar, transition, and turbulent-flow regions, Aiche J. 1 (4) (1955) 434–440.
[23] J.P. Solano, A. García, P.G. Vicente, A. Viedma, Flow field and heat transfer investigation in tubes of heat exchangers with motionless scrapers, Appl. Therm. Eng. 31 (2011) 2013–2024, https://doi.org/10.1016/j.applthermaleng.2011.03.010. <http://www.sciencedirect.com/science/article/pii/S1359431111001426> .
[24] J.P. Solano, A. García, P.G. Vicente, A. Viedma, Flow pattern assessment in tubes of reciprocating scraped surface heat exchangers, Int. J. Therm. Sci. 50 (2011) 803–815, https://doi.org/10.1016/j.ijthermalsci.2010.11.019. <http://www.sciencedirect.com/science/article/pii/S1290072910003315> .
[25] K. Sun, D. Pyle, A. Fitt, C. Please, M. Baines, N. Hall-Taylor, Numerical study of 2D heat transfer in a scraped surface heat exchanger, Comput. Fluids 33 (2004) 869–880.
[26] W. Wang, J. Walton, K. McCarthy, Flow profiles of Power Law fluids in scraped surface heat exchanger geometry using MRI, J. Food Process. Eng. 22 (1999) 11–27.
[27] R. Webb, Performance evaluation criteria for use of enhanced heat transfer surface in heat exchanger design, Int. J. Heat Mass Transfer 24 (1981) 715–726.
[28] X.H. Yang, W.L. Zhu, Viscosity properties of sodium carboxymethylcellulose solutions, Cellulose (2007), https://doi.org/10.1007/s10570-007-9137-9. <http://www.springerlink.com/content/f84527kqx3w508t1/>.
[29] M. Yataghene, F. Fayolle, J. Legrand, Experimental and numerical analysis of heat transfer including viscous dissipation in a scraped surface heat exchanger, Chem. Eng. Process. 48 (2009) 1447–1458, https://doi.org/10.1016/j.cep.2009.07.012. <http://www.sciencedirect.com/science/article/pii/S0255270109001500> .
[30] M. Yataghene, F. Francine, L. Jack, Flow patterns analysis using experimental PIV technique inside scraped surface heat exchanger in continuous flow condition, Appl. Therm. Eng. 31 (2011) 2855–2868, https://doi.org/10.1016/j.applthermaleng.2011.05.011. <http://www.sciencedirect.com/science/article/pii/S1359431111002638> .
[31] M. Yataghene, J. Pruvost, F. Fayolle, J. Legrand, CFD analysis of the flow pattern and local shear rate in a scraped surface heat exchanger, Chem. Eng. Process. 47 (2008) 1550–1561, https://doi.org/10.1016/j.cep.2007.07.009. <http://www.sciencedirect.com/science/article/pii/S0255270107002292> .